Relay Mobility

Submitted in partial fulfillment of
the requirements for the degree of

Bachelor of Technology
in Electrical Engineering
&
Master of Technology
in Communications and Signal Processing

by

Prudhvi Porandla
110070039

Under the guidance of
Prof. S. N. Merchant

Department of Electrical Engineering
Indian Institute of Technology Bombay
2016

Dissertation Approval

The dissertation entitled *TITLE* by *Prudhvi Porandla (110070039)* is approved for the degree of *Bachelor of Technology* in *Electrical Engineering* and *Master of Technology* in *Communications and Signal Processing.*

.....	.....
Examiner	Examiner
.....	.....
Supervisor	Chairman

Date: June 20, 2016

Place: IIT Bombay

Declaration

I declare that this written submission represents my ideas in my own words and wherever others' ideas or words have been included, I have adequately cited and referenced the original sources. I also declare that I have adhered to all principles of academic honesty and integrity and have not misrepresented or fabricated or falsified any idea/ data/ fact/ source in my submission. I understand that any violation of the above will be cause for disciplinary action by IIT Bombay and can also evoke penal action from the sources which have thus not been properly cited or from whom proper permission has not been taken when needed.

Prudhvi Porandla

Date: June 20, 2016

Place: IIT Bombay

To YOU

Acknowledgements

I would like to express my sincere gratitude to my supervisor Prof. S. N. Merchant for his invaluable guidance throughout the three years of my association with him. They have always been accessible and willing to clear my doubts and have provided valuable insights that helped me develop new ways to approach the problem and come up with better solutions.

June 20, 2016 Prudhvi Porandla

Abstract

We explore the application of compressed sensing for solving problems in radio astronomy where the source images are generally sparse in some domain. We obtain an incomplete set of noisy Fourier measurements of the image through the radio telescope array and the goal is to reconstruct the image by making use of the sparse nature of the images.

In this report we consider the case where we have multiple sets of Fourier measurements corresponding to different images and in addition we have some knowledge about some overlapping information between the images. By making use of the overlapping information we should be able to perform better reconstruction than in the case where we perform the reconstruction for the images independently.

We propose a coupled formulation where we solve a joint minimization problem to perform simultaneous recovery of multiple images. We restrict ourselves to the case where we have two images and present an alternating algorithm that solves the joint minimization problem.

We conduct experiments on different classes of images that include images that are sparse in spatial domain, images that are sparse in wavelet domain and images that are sum of a spatial domain sparse component and a wavelet domain sparse component. In all the cases we observed that the coupled formulation that does simulataneous recovery has better performance as compared to when we perform the reconstructions independently.

Contents

List of Figures

Chapter 1

Introduction

The broad goal of the field of signal processing is to reconstruct a signal and gain insights into its characteristics based on a series of sampling measurements obtained at discrete time intervals. For a general signal, this task is impossible due to non-availability of data in between two sampling intervals. But, with some prior information about the signal, measurements can be conducted in appropriate ways that enable reconstruction of signals to the desired accuracy.

For example, for a smooth signal which varies slowly with time, sample and hold type of measurements can be conducted to reconstruct the signal to the required accuracy. For another category of signals namely bandlimited signals, the Nyquist-Shannon sampling theorem was an important breakthrough in the field of signal processing. The Nyquist-Shannon sampling theorem states that perfect reconstruction is possible from a set of uniformly spaced samples taken at the Nqyuist rate of twice the highest frequency present in the signal.

Unfortunately, in many applications it may be too costly or physically impossible to build devices capable of sampling at the Nyquist rate or even if it is possible we may end up with far too many samples to efficiently store and process. To address the challenges involved in dealing with such high dimensional data we often depend on compression, which aims to find the most concise representation of a signal that is able to achieve a target level of distortion. Transform coding, one of the most popular techniques for signal compression, relies on finding a basis or a frame that provides sparse or compressible representations for signals in a class of interest. Both sparse and compressible signals can be represented with high fidelity by preserving only the the values and locations of the

largest k coefficients of the signals, where $k \ll n$, and n is the length of the signal.

Compressed sensing is a framework for signal acquisition and sensor design that enables a potentially large reduction in the sampling and computation costs for sensing signals that have a sparse or compressible representation. The fundamental idea behind compressed sensing is rather than first sampling at a higher rate and then compressing sampled data, we would like to directly sense the data in compressed form at a much lower sampling rate. The field of compressed sensing grew out of the work of Candes, Tao and Romberg who showed that, a finite-dimensional signal having a sparse or compressible representation can be recovered from a much smaller number of linear measurements than what Nyquist rate sampling demands [1, 2, 3]. Compressed sensing methods are fast and highly configurable, which makes them highly attractive for a lot of problems such as improving MRI imaging [2], developing single pixel cameras [4], face recognition algorithms etc. However compressed sensing is still a recent field and its applicability to a large number fields has not yet been fully studied. Basic information on compressed sensing can be obtained from [5]. For a complete up-to-date review on compressed sensing refer to [6]. As a part of this thesis, we study the application of compressed sensing methods for improving radio astronomy imaging techniques.

Compressed Sensing and Radio Astronomy

Radio Astronomy studies celestial objects at radio frequencies around the metre wavelength, by utilizing the techniques of radio interferometry and aperture synthesis. Mathematically, the problem is equivalent to reconstructing the image of the astronomical object from incomplete and noisy Fourier measurements of the image. From the theory of compressed sensing we know that such measurements may actually suffice for accurate reconstruction of the image provided that the image is sparse in some domain.

Our earlier work [7] focused on applying compressed sensing techniques to recover an image of astronomical sources from a an incomplete set of its Fourier measurements. Also, we analyzed the optimality of the GMRT telescope [8] with respect to reconstruction using compressed sensing techniques and came up with optimal antenna locations for additions to the array.

In this project we consider the case where we have two sets of Fourier measurements

corresponding to two different images but in addition we have knowledge about some overlapping information between the two images. The goal is to use this additional information and perform simultaneous recovery of both images that performs better than if we reconstruct the images independently. We propose an alternating algorithm that performs simultaneous recovery by solving a joint minimization problem and then conduct experiments to compare the results of the alternating algorithm with those obtained from independent reconstructions.

Organization of the report

The organization of the report is as follows:

1. **Chapter 2** introduces radio astronomy and the basics of radio imaging techniques such as radio interferometry and aperture synthesis.

2. **Chapter 3** presents the mathematical model for the compressed sensing problem in a simultaneous recovery setting. We present an alternating algorithm to solve the joint minimization problem to perform simultaneous recovery.

3. **Chapter 4** analyzes the experiments conducted on simulated data. In this chapter the performance of the alternating algorithm that performs simultaneous recovery is compared against that of the algorithm that reconstructs images separately.

4. **Conclusion and Further Work**

We use stochastic geometry to analyze the performance of a partial decode-and-forward (PDF) relaying scheme applied in a user-assisted relaying setting, where an active user relays data through another idle user in uplink cellular communication. We present the geometric model of a network deploying user-assisted relaying and propose two geometric cooperation policies for fast and slow fading channels. We analytically derive the cooperation probability for both policies. This cooperation probability is further used in the analytical derivation of the moments of inter-cell interference power caused by system-wide deployment of this user-assisted PDF relaying. We then model the inter-cell interference power statistics using the Gamma distribution by matching the first two moments analytically derived. This cooperation and interference analysis provides the

theoretical basis for quantitatively evaluating the performance impact of user-assisted relaying in cellular networks. We then numerically evaluate the average transmission rate performance and show that user-assisted relaying can significantly improve per-user transmission rate despite the increased inter-cell interference. This transmission rate gain is significant for active users near the cell edge and further increases with higher idle user density, supporting user-assisted relaying as a viable solution to crowded population areas.

1.1 Introduction

1.1.1 Motivation

Mobile subscribers operators and continual driven customer by the increasing demand for number new and of better services place pressing requirements on the underlying wireless technologies to provide high data rates and wide coverage. Future generation networks that promise higher data rates and multifold increase in system capacity include 3GPP Long Term Evolution-Advanced (LTE-A, 4G) and the emerging 5G systems. The fourth generation (4G) wireless systems were designed to fulfill the requirements of the International Mobile Telecommunications - Advanced (IMT-A). LTE as a practical 4G wireless system has been recently deployed in some countries and LTE-A is expected to be deployed soon around the globe. It is well established that 4G networks have just reached the theoretical limit on the data rate with current technologies. These technologies are being complemented in the fifth generation (5G) wireless systems by designing and developing new radio concepts to accommodate higher data rates, larger network capacity, higher energy efficiency, and higher mobility necessary to meet the new and challenging requirements of new wireless applications. 5G wireless systems are expected to support peak data rate of 10 Gb/s for low mobility and 1 Gb/s for high mobility. These networks are expected to be standardized and deployed around and beyond 2020. Various promising technologies are proposed for 5G wireless communication systems such as massive MIMO, energy-efficient communications, Device-to- Device (D2D) communications, millimeter-wave (mmWave), and cognitive radio networks.

D2D and Relaying cooperative communications will play important roles in future generations wireless networks. D2D communications enable two proximity users to transmit

signal directly without going through the base station; subsequently, 5G wireless systems are expected to relax the restrictions on the need to route all user data through the core network. D2D communications can increase network spectrum utilization and energy efficiency, reduce transmission delay, offload traffic for the base station, and alleviate congestion in the cellular core networks, which make it a promising technology for future wireless systems. Relay-aided cooperative communi- cation techniques represent another promising technology that improves performance in poor coverage areas by enabling ubiquitous coverage even for users in the most unfavorable channel conditions. The latest release of the LTE standard allows the deployment of fixed wireless relays to help cell- edge mobiles. Yet, other advanced cellular relaying modes are expected in 5G systems to improve the topology and robustness of a cellular network and decrease power consumption. These new technologies include mobile relaying, multi-hop relaying, and user-equipment based (user-assisted) relaying enabled by D2D communications

1.1.2 Organization of this report

This report is in further divided into 6 sections. The topics are organized as follows.

Section 2 will discuss partial decode and forward relaying in a standalone setup. The two phases of transmission, signal design and achievable rate of the scheme are presented.

Section 3 is about deployment of the relaying scheme discussed in section 2 in a cellular network. Inter-cell interference and equivalent standard channel model are discussed.

Section 4 contains policies to determine whether the nearest idle neighbour to the active UE can be picked as a relay. Two policies were proposed and analytic expressions for cooperation probabilities were derived.

Section 5 Analytic expressions for interference powers were developed and shape and scale parameters of Gamma distribution that fits interference power statistics were calculated.

Section 6 discusses the simulation setting and how it is different from the theoritical method and the values of parameter used in simulation were listed. It also has simulation results with brief explanations of the result.

Section 7 lists three different topics I'm planning to work on during the second phase. All links/references to equation or figures in this report are clickable.

1.2 Partial Decode-and-Forward Relaying

In this section, we discuss the signal design, channel model and achievable rate of PDF relaying scheme.

1.2.1 Signal Design

Consider a source $\mathcal{S}$, its relay $\mathcal{R}$ and the destination $\mathcal{D}$. Each transmission block is divided into two phases: 1. broadcast transmission in which $\mathcal{S}$ broadcasts to both $\mathcal{R}$ and $\mathcal{D}$. 2. multiple access transmission in which both $\mathcal{S}$ and $\mathcal{R}$ transmit to $\mathcal{D}$. In each block of transmission, $\mathcal{S}$ splits its information into a common part and a private part. The common part is encoded via U_s^b in the 1st phase and $U_s^{m_1}$ in the 2nd phase; and the private part is encoded via $V_s^{m_2}$ in the 2nd phase. The relay $\mathcal{R}$ decodes the information sent by $\mathcal{S}$ in first phase and encodes the same information using $U_s^{m_1}$ in the 2nd phase.

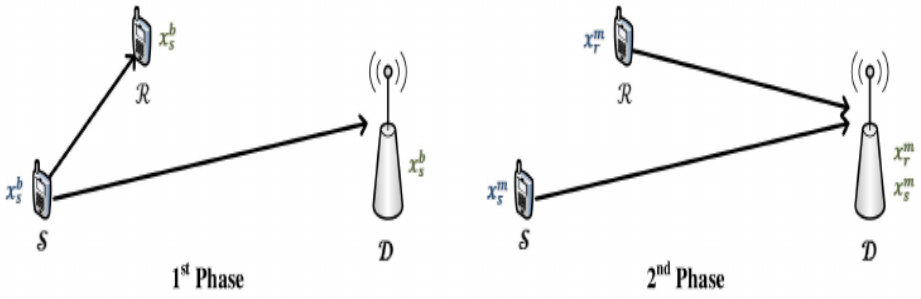

Figure 1.1: Transmission phases in PDF relaying

The signals transmitted by $\mathcal{R}$ and $\mathcal{S}$ are as follows:

$$\text{Phase 1:} \quad x_s^b = \sqrt{P_s^b} U_s^b, \tag{1.1}$$

$$\text{Phase 2:} \quad x_r^m = \sqrt{P_r^m} U_s^{m_1}, \tag{1.2}$$

$$x_s^m = \sqrt{P_s^{m_1}} U_s^{m_1} + \sqrt{P_s^{m_2}} V_s^{m_2} \tag{1.3}$$

All codewords above are picked from independent Gaussian codebooks with zero mean and unit variance.

Power Constraints: Let P_s and P_r be the transmit powers of $\mathcal{S}$ and $\mathcal{R}$ respectively and α_1 be the fraction of transmission time allocated to first phase, then the following average power constraints should to be satisfied:

$$\alpha_1 P_s^b + \alpha_2 P_s^m = P_s, \quad \alpha_2 P_r^m = P_r \tag{1.4}$$

where $\alpha_2 = 1 - \alpha_1$

1.2.2 Channel Model

Considering the transmit signals presented above and assuming flat fading over the two phases, the received signals at $\mathcal{R}$ and $\mathcal{D}$ during first phase are

$$Y_r^b = h_{sr} x_s^b + Z_r^b, \quad Y_d^b = h_{sd} x_s^b + Z_d^b \tag{1.5}$$

where b denotes broadcast mode, Z_r^b and Z_d^b are $i.i.d$ circularly-symmetric complex gaussians with mean 0 and variance σ^2 - $\mathcal{CN}(0, \sigma^2)$ that represent noises at $\mathcal{R}$ and $\mathcal{D}$.
Similarly the received signal at $\mathcal{D}$ during second phase can be modelled as

$$Y_d^m = h_{sd} x_s^m + h_{rd} x_r^m + Z_d^m \tag{1.6}$$

here m denotes multicast transmission; all others have usual meaning. The above expression is true only if $\mathcal{D}$ has knowledge about the phase offset between $\mathcal{S}$ and $\mathcal{R}$. This assumption is justified by noting that the phase offset between the two nodes can be estimated at base station.

1.2.3 Achievable Rate

With transmit signals in equations 1.1- 1.3 and joint ML decoding rule at $\mathcal{D}$, the achievable rate for this relaying scheme is:

$$R_{PDF} \leq min(C_1 + C_2, C_3) \tag{1.7}$$

$$\text{where } C_1 = \alpha_1 \log\left(1 + |h_{sr}|^2 P_s^b\right), \tag{1.8}$$

$$C_2 = \alpha_2 \log\left(1 + |h_{sd}|^2 P_s^{m_2}\right), \tag{1.9}$$

$$C_3 = \alpha_1 \log\left(1 + |h_{sd}|^2 P_s^b\right) + \alpha_2 \log\left(1 + |h_{sd}|^2 P_s^{m_2} + \left(|h_{sd}|\sqrt{P_s^{m_1}} + |h_{rd}|\sqrt{P_r^m}\right)^2\right) \tag{1.10}$$

C_1 represents the rate of the common part that can be decoded at $\mathcal{R}$, C_2 the private part that can be decoded at $\mathcal{D}$ provided the common part has been decoded correctly, and C_3 both the common and private parts that can be jointly decoded at $\mathcal{D}$. These rates are achievable provided full CSI at all receivers and the source-relay phase offset knowledge.

Now that we know what PDF relaying scheme is and the achievable rate, let us see how this scheme performs in cellular networks. To analyse system performance under PDF relaying, we need to know network geometry i.e., how the users and base stations are distributed, how many users can take advantage of relaying, how users identify a potential relay etc. In the next couple of sections we describe network geometry, received signals and interference model when relaying is deployed in the whole network, and cooperation policies.

1.3 Cellular Network Geometry and User-Assisted Relaying

1.3.1 Network geometry model

Consider a cellular system which consists of multiple cells, each cell has a single base station and each base station serves multiple users. Each of the users uses a distinct frequency block. Each user is served by the single base station that is closest to that user.

We use stochastic geometry to describe the uplink cellular network. We assume that the active users in different cells that use the same resource block and cause interference to each other are distributed on a two-dimensional plane according to a homogeneous and stationary Poisson point process (PPP) Φ_1 with intensity λ_1. The set of user equipments(UEs) that are in idle state and can participate in relaying are distributed according to another PPP Φ_2 with intensity λ_2. We assume Φ_1 and Φ_2 are independent. Further-

more, under the assumption that each BS serves a single mobile in a given resource block, the BS should be closer to its served UE than to any other UE. Therefore we assume each BS is uniformly distributed in the Voronoi cell of its served UE. Fig. 1.2 shows an example layout of the network.

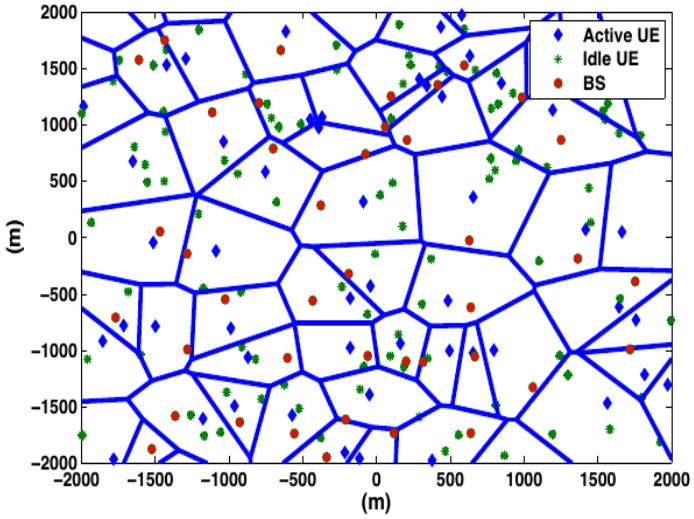

Figure 1.2: Sample layout of a cellular network ($\lambda_2 = 2\lambda_1$)

1.3.2 Channel Model

In this section, we describe the channel model when PDF relaying is deployed in cellular network. In this case, there will be out-of-cell inteference in addition to noise. The interference is due to frequency reuse in other cells.

Consider i^{th} active UE, we model the received signals at the relay and base station in this cell during 1st phase as

$$Y^b_{r,i} = h^{(i)}_{sr} x^b_{s,i} + I^b_{r,i} + Z^b_{r,i},$$

$$Y^b_{d,i} = h^{(i)}_{sd} x^b_{s,i} + I^b_{d,i} + Z^b_{d,i} \tag{1.11}$$

where $I^b_{r,i}$ and $I^b_{d,i}$ represent the interference received at the i^{th} relay and destination.

In second phase of the transmission, the received signal at the BS can be modelled as

$$Y^m_{d,i} = h^{(i)}_{sd} x^m_{s,i} + h^{(i)}_{rd} x^m_{r,i} + I^m_{d,i} + Z^m_{d,i} \tag{1.12}$$

1.3.3 Interference

To model interference, we assume prefect frame synchronization. LTE-Advanced imposes very strict requirements on synchronization anyway. Interference at the relay during first phase and at the destination(BS) during first and second phases can be expressed as

$$I_{r,i}^{b} = \sum_{k \neq i} B_k h_{sr}^{(k,i)} x_{s,k}^{b} + (1 - B_k) h_{sr}^{(k,i)} x_{s,k},$$

$$I_{d,i}^{b} = \sum_{k \neq i} B_k h_{sd}^{(k,i)} x_{s,k}^{b} + (1 - B_k) h_{sd}^{(k,i)} x_{s,k},$$

$$I_{d,i}^{m} = \sum_{k \neq i} B_k \left(h_{sd}^{(k,i)} x_{s,k}^{m} + h_{rd}^{(k,i)} x_{r,k}^{m} \right) + (1 - B_k) h_{sd}^{(k,i)} x_{s,k} \tag{1.13}$$

the summation is over all active users. Here, $h_{sd}^{(k,i)}$ and $h_{rd}^{(k,i)}$, respectively, are the channel fading from the k^{th} active UE in Φ_1 and the associated relaying UE in Φ_2 to the BS associated with the i^{th} active UE in Φ_1; and $h_{sr}^{(k,i)}$ is the channel fading from the k^{th} active UE in Φ_1 to the relaying UE associated with the i^{th} active UE in Φ_1.

B_k in above expressions is a Bernoulli random variable with success probability ρ. $B_k = 1$ is used to indicate the k^{th} active UE's decision to exploit the help of another idle UE, a relay, and apply the relaying transmission strategy, and $B_k = 0$ indicates that the k^{th} UE has no relay. In section 1.4, we derive the cooperation probability ρ for different cooperation policies.

For a given setting of nodes locations, based on the interference model in Eq. 1.13, we can use the fact that interference at either the relay or destination is the sum of an infinite number of signals undergoing independent fading from nodes distributed in the infinite 2-D plane and use the law of large numbers to approximate the interference as a complex Gaussian distribution. Also, since the transmitted codewords are complex Gaussian with zero mean, mean of interference is zero. To fully characterize interference as a complex Gaussian distribution, we define their distributions as $I_{d,i}^{b} \sim \mathcal{CN}(0, \mathcal{Q}_{d,i}^{b}), I_{d,i}^{m} \sim \mathcal{CN}(0, \mathcal{Q}_{d,i}^{m})$, and $I_{r,i}^{b} \sim \mathcal{CN}(0, \mathcal{Q}_{r,i})$ with the variances derived later in Section 1.5. The power of these interference terms which correspond to the variance of the Gaussian random variables are function of node locations and hence vary with

different network realizations.

1.3.4 Equivalent Standard Channel Model

Using the interference model discussed above, we can convert the channel model in case of relaying into the standard form to capture the effects of interference into the channel fading as

$$\tilde{Y}_{r,i}^{b} = \tilde{h}_{sr}^{(i)} x_{s,i}^{b} + \tilde{Z}_{r,i}^{b},$$
$$\tilde{Y}_{d,i}^{b} = \tilde{h}_{sd}^{(i)} x_{s,i}^{b} + \tilde{Z}_{d,i}^{b},$$
$$\tilde{Y}_{d,i}^{m} = \tilde{h}_{sd}^{(i)} x_{s,i}^{m} + \tilde{h}_{rd}^{(i)} x_{r,i}^{m} + \tilde{Z}_{d,i}^{m}$$

where the new channel fading terms are defined as

$$\tilde{h}_{sr}^{(i)} = \frac{h_{sr}^{(i)}}{\sqrt{\mathcal{Q}_{r,i} + \sigma^2}}, \quad \tilde{h}_{sd}^{(b,i)} = \frac{h_{sd}^{(i)}}{\sqrt{\mathcal{Q}_{d,i}^{b} + \sigma^2}} \quad \tilde{h}_{sd}^{(m,i)} = \frac{h_{sd}^{(i)}}{\sqrt{\mathcal{Q}_{d,i}^{m} + \sigma^2}}, \quad \tilde{h}_{rd}^{(i)} = \frac{h_{rd}^{(i)}}{\sqrt{\mathcal{Q}_{d,i}^{m} + \sigma^2}}$$

and the noise terms are now all $\mathcal{CN}(0, 1)$. Using these equivalent standard channels, we can compute the transmission rate using Eq. 1.7

1.4 Cooperation Policies and Probability

In this section, we look at three cooperation policies: an ideal policy E_1, a pure geometric policy E_2 and a hybrid policy E_3 that defines whether an active UE should select an inactive UE to use it in PDF relaying. Also, expressions for cooperation probabilities of E_2 and E_3 are derived.

1.4.1 Policies

Ideal Policy E_1

The ideal cooperation policy E_1 requires the active UE nodes to know instantaneous SINRs of the relay link($\mathcal{S}-\mathcal{R}$) and the direct link($\mathcal{S}-\mathcal{D}$). The policy is defined as

$$E_1 = \left\{ |\tilde{h}_{(sr)}^{(k)}|^2 \geq |\tilde{h}_{(sd)}^{(k)}|^2 \right\}$$
$$\backsimeq \left\{ \frac{g_{sr} r_2^{-\alpha}}{\mathcal{Q}_{r,k}} \geq \frac{g_{sd} r_1^{-\alpha}}{\mathcal{Q}_{d,k}^b} \right\}$$

where r_1 and r_2 denote the direct distance between $\mathcal{S}$ and $\mathcal{D}$ and cooperation distance between $\mathcal{S}$ and its closest idle UE, respectively and α is pathloss exponent. This event E_1 identifies whether an idle UE will be associated as a relay for the k^{th} UE and participate in transmission. Noise variance σ^2 is ignored since interference power dominates.

Since interference at relay and destination during first phase is more or less the same and g_{sr}, g_{sd} are identically distributed, we can safely ignore them and propose a policy that depends only on distances.

Pure Geometric Policy E_2

This policy is defined as

$$E_2 = \{r_2 \leq r_1, D \leq r_1\} \tag{1.14}$$

where D is the distance between $\mathcal{R}$ and $\mathcal{D}$. In words, if source's(active UE's) nearest idle neighbour is in the intersection region of two circles of radius r_1 centered at source and destination, then that idle UE will be chosen to act as a relay.

E_2 is more practical than policy E_1 in the sense that it does not require full knowledge of both the channel fading and the interference at the decision making node. Instead, it only requires the decision making nodes to know the distances from the active user to the nearest idle user and to the base station. It represents a practical decision making strategy for fast fading channels, requiring no knowledge of the channel fading.

Hybrid Policy E_3

This policy is proposed for slow fading channels where small scale fading parameters estimation and their feedback to the decision making node is feasible.

$$E_3 = \{g_{sd} r_1^{-\alpha} \leq g_{sr} r_2^{-\alpha}, D \leq r_1\} \tag{1.15}$$

Note that this cooperation policy is still independent of the interference as in the pure geometric cooperation policy E_2.

1.4.2 Cooperation Probabilities

In this part of the section we derive cooperation probabilities ρ_2 and ρ_3 for the policies E_2 and E_3 respectively. For the ideal policy E_1, analytic evaluation of the cooperation probability is rather complicated because of the inter-dependency between the cooperation decision and consequential interference among different cells. Consider a random BS and its associated active UE. The distribution of the distance r_1 between the i^{th} UE and its associated BS can be shown to be Rayleigh distributed directly from the null probability of a two dimensional PPP distribution.

Due to the stationarity of the PPP, i.e., location of the origin doesn't change the distribution of points, and the independence of Φ_2 from BSs distribution we can assume that the location of the UE associated with the BS under study represents the origin point of Φ_2 . Then, each UE in Φ_1 chooses the closest UE in Φ_2 to assist it in relaying its message to the serving BS. Hence, similar to source-to- destination distance, the distribution of the source-to-relay distance r_2 between the i^{th} UE and its associated relaying UE can be also shown to be Rayleigh distributed from the null probability of a two dimensional PPP. Therefore,

$$f_{r_1}(r_1) = 2\pi\lambda_1 r_1 e^{-\lambda_1 \pi r_1^2},$$

$$f_{r_2}(r_2) = 2\pi\lambda_2 r_2 e^{-\lambda_2 \pi r_2^2} \tag{1.16}$$

Theorem 1.1. *Cooperation Probabilities. The probability of deploying user-assisted relaying for a randomly located active user within a cell can be evaluated as follows:*

i. For policy E_2

$$\rho_2 = \int_{-\pi/2}^{-\pi/3} \frac{2\lambda_2 cos^2\psi_0}{\pi(\lambda_1 + 4\lambda_2 cos^2\psi_0)} d\psi_0 + \int_{\pi/3}^{\pi/2} \frac{2\lambda_2 cos^2\psi_0}{\pi(\lambda_1 + 4\lambda_2 cos^2\psi_0)} d\psi_0 + \frac{\lambda_2}{3(\lambda_1 + \lambda_2)} \tag{1.17}$$

ii. For policy E_3

$$\begin{aligned}
\rho_3 = & \int_0^2 f_\beta(z) \int_{-\pi/2}^{-cos^{-1}(z/2)} \frac{2\lambda_2 cos^2\psi_0}{\pi(\lambda_1 + 4\lambda_2 cos^2\psi_0)} d\psi_0 dz \\
& + \int_0^2 f_\beta(z) \int_{cos^{-1}(z/2)}^{\pi/2} \frac{2\lambda_2 cos^2\psi_0}{\pi(\lambda_1 + 4\lambda_2 cos^2\psi_0)} d\psi_0 dz \\
& + \int_0^2 f_\beta(z) \frac{\lambda_2 z^2 cos^{-1}(z/2)}{\pi(\lambda_1 + \lambda_2 z^2)} dz \\
& + \int_2^\infty f_\beta(z) \int_{-\pi/2}^{\pi/2} \frac{2\lambda_2 cos^2\psi_0}{\pi(\lambda_1 + 4\lambda_2 cos^2\psi_0)} d\psi_0 dz
\end{aligned}$$

where $\beta = \left(\frac{g_{sr}}{g_{sd}}\right)^{1/\alpha}$ *and* $f_\beta(z)$ *is pdf of* β *which can be shown to be*

$$f_\beta(z) = \frac{\alpha z^{\alpha-1}}{(1+z^\alpha)^2} \tag{1.18}$$

Proof. i.

$$\begin{aligned}
\rho_2 &= \mathbb{P}\{E_2\} \\
&= \mathbb{P}\{r_2 \le r_1, r_1^2 + r_2^2 - 2r_1 r_2 cos\psi_0 \le r_1^2\} \\
&= \mathbb{P}\{r_2 \le r_1, r_2 \le 2r_1 cos\psi_0\}
\end{aligned}$$

when $|\psi_0| < \pi/3,\ r_1 < 2r_1 cos\psi_0 \Rightarrow$ if $r_2 < r_1$, r_2 satisfies both inequalities. Accordingly, we define $\mathcal{E}_1$ and $\mathcal{E}_2$ as follows

$$\begin{aligned}
\mathcal{E}_1 &= (2\pi)^2 \lambda_1 \lambda_2 \int_0^\infty \int_0^{2r_1 cos\psi_0} r_1 r_2 e^{-\pi(\lambda_1 r_1^2 + \lambda_2 r_2^2)} dr_2 dr_1 \\
&= \frac{2\lambda_2 cos^2\psi_0}{\pi(\lambda_1 + 4\lambda_2 cos^2\psi_0)} \\
\mathcal{E}_2 &= (2\pi)^2 \lambda_1 \lambda_2 \int_0^\infty \int_0^{r_1} r_1 r_2 e^{-\pi(\lambda_1 r_1^2 + \lambda_2 r_2^2)} dr_2 dr_1 \\
&= \frac{\lambda_2}{2\pi(\lambda_1 + \lambda_2)}
\end{aligned}$$

$$\text{Now, } \rho_2 = \int_{-\pi/3}^{\pi/3} \mathcal{E}_2 d\psi_0 + 2\int_{\pi/3}^{\pi/2} \mathcal{E}_1 d\psi_0$$
$$= \frac{\lambda_2}{3(\lambda_1+\lambda_2)} + 2\int_{\pi/3}^{\pi/2} \mathcal{E}_1 d\psi_0$$

ii.

$$\rho_3 = \mathbb{P}\{E_3\} \tag{1.19}$$
$$= \mathbb{P}\{r_2 \leq \left(\frac{g_{sr}}{g_{sd}}\right)^{1/\alpha} r_1, r_1^2 + r_2^2 - 2r_1 r_2 cos\psi_0 \leq r_1^2\} \tag{1.20}$$
$$= \mathbb{P}\{r_2 \leq \beta r_1, r_2 \leq 2r_1 cos\psi_0\} \tag{1.21}$$
$$= \mathbb{P}\{r_2 \leq 2r_1 cos\psi_0\} \qquad \text{for } \beta > 2 \tag{1.22}$$
$$= \mathbb{P}\{r_2 \leq \beta r_1\} \qquad \text{for } \beta < 2 \text{ and } |\psi_0| < cos^{-1}(\beta/2) \tag{1.23}$$
$$= \mathbb{P}\{r_2 \leq 2r_1 cos\psi_0\} \qquad \text{for } \beta < 2 \text{ and } cos^{-1}(\beta/2) < |\psi_0| < \pi/2 \tag{1.24}$$
$$\therefore \rho_3 = 2\int_0^2 f_\beta(z) \int_{cos^{-1}(z/2)}^{\pi/2} \mathcal{E}_1 d\psi_0 dz + \int_0^2 f_\beta(z) \int_{-cos^{-1}(z/2)}^{cos^{-1}(z/2)} \mathcal{E}_3 d\psi_0 dz \tag{1.25}$$
$$+ \int_2^\infty f_\beta(z) \int_{-\pi/2}^{\pi/2} \mathcal{E}_1 d\psi_0 dz \tag{1.26}$$

$\mathcal{E}_1$ is defined in part i. of the proof and $\mathcal{E}_3 = \frac{\lambda_2 z^2}{2\pi(\lambda_1+\lambda_2 z^2)}$ which is nothing but $\mathcal{E}_2$ with $\lambda_2 = \lambda_2 z^2$. $f_\beta(z)$, the pdf of β, can be obtained as follows

$$F_\beta(z) = \mathbb{P}\left\{\left(\frac{x_1}{x_2}\right)^{1/\alpha} \leq z\right\} = \mathbb{P}\{x_1 \leq z^\alpha x_2\}$$
$$= \int_0^\infty \int_0^{z^\alpha x_2} e^{-(x_1+x_2)} dx_1 dx_2 \quad \text{since } g_{sr}, g_{sd} \sim Exp(1)$$
$$= 1 - \frac{1}{1+z^\alpha}, \qquad z \in [0,\infty)$$

The pdf $f_\beta(z)$ is then obtained by differentiating $F_\beta(z)$:

$$f_\beta(z) = \frac{dF_\beta(z)}{dz} = \frac{\alpha z^{\alpha-1}}{(1+z^\alpha)^2} \quad z \in [0,\infty)$$

□

1.5 Interference Analysis

User-assisted relaying actually increases the amount of out- of-cell interference in the network as some idle users are now transmitting when relaying information of active users. It is therefore necessary to understand this out-of-cell interference power, particularly its distribution, in order to assess the overall impact of user-assisted relaying on system performance.

1.5.1 First Two Moments of Interference Power

Since it is difficult to describe the exact distribution of out-of-cell interference power, here we choose to model the interference power to the cell under study as a Gamma distribution by fitting the first two moments of the interference power analytically developed using stochastic geometry of the field of interferers outside that cell. The expressions for interference power can be developed from Eqs. 1.13.

$$\mathcal{Q}^b_{d,i} = \sum_{k\neq i} B_k \left|h^{(k,i)}_{sd}\right|^2 P^b_{s,k} + (1-B_k)\left|h^{(k,i)}_{sd}\right|^2 P_{s,k} \tag{1.27}$$

$$\mathcal{Q}^m_{d,i} = \sum_{k\neq i} \left[B_k\left(\left|h^{(k,i)}_{sd}\right|^2 P^m_{s,k} + \left|h^{(k,i)}_{rd}\right|^2 P^m_{r,k}\right)\right] + (1-B_k)\left|h^{(k,i)}_{sd}\right|^2 P_{s,k} \tag{1.28}$$

$$\mathcal{Q}_{r,i} = \sum_{k\neq i} B_k \left|h^{(k,i)}_{sr}\right|^2 P^b_{s,k} + (1-B_k)\left|h^{(k,i)}_{sr}\right|^2 P_{s,k} \tag{1.29}$$

Theorem 1.2. *Interference Power Statistics For network-wide deployment of user-assisted relaying, the out-of-cell interfer- ence generated at the destination BS and the relaying UE have the following statistics:*

i. The first two moments, mean and variance, of interference power at the destination BS during the 1st and 2nd phase, respectively, are

$$\mathbb{E}[\mathcal{Q}^b_{d,i}] = \frac{2\pi\lambda_1\zeta_1}{\alpha-2}R_c^{2-\alpha}, \qquad \mathbb{E}[\mathcal{Q}^m_{d,i}] = \frac{2\pi\lambda_1\zeta_3}{\alpha-2}R_c^{2-\alpha} \tag{1.30}$$

$$var[\mathcal{Q}^b_{d,i}] = \frac{\pi\lambda_1\zeta_2}{\alpha-1}R_c^{2(1-\alpha)}, \qquad var[\mathcal{Q}^m_{d,i}] = \frac{\pi\lambda_1\zeta_4}{\alpha-1}R_c^{2(1-\alpha)} \tag{1.31}$$

ii. The first two moments, mean and variance, of interfer- ence power at the idle UE

associated as a relay with the ith active UE are

$$\mathbb{E}[\mathcal{Q}_{r,i}] = \lambda_1 \zeta_1 \int_0^{2\pi} \int_{R_c}^{\infty} (r^2 + D^2 - 2rDcos\theta)^{\alpha/2} r dr d\theta \tag{1.32}$$

$$var[\mathcal{Q}_{r,i}] = \lambda_1 \zeta_2 \int_0^{2\pi} \int_{R_c}^{\infty} (r^2 + D^2 - 2rDcos\theta)^{\alpha/2} r dr d\theta \tag{1.33}$$

$$\begin{aligned} where \quad \zeta_1 &= \rho_1 P_{s,k}^b + (1-\rho_1) P_{s,k} && (1.34)\\ \zeta_2 &= 2[\rho_1 (P_{s,k}^b)^2 + (1-\rho_1) P_{s,k}^2], && (1.35)\\ \zeta_3 &= \rho_1 (P_{s,k}^m + P_{r,k}^m) + (1-\rho_1) P_{s,k}, && (1.36)\\ \zeta_4 &= 2[\rho_1 (P_{s,k}^m + P_{r,k}^m)^2 + (1-\rho_1) P_{s,k}^2 - \rho_1 P_{s,k}^m P_{r,k}^m] && (1.37) \end{aligned}$$

Proof.

$$\begin{aligned} \mathbb{E}[\mathcal{Q}_{d,i}^b] &= -\frac{\partial \mathcal{L}_{\mathcal{Q}_{d,i}^b}(s)}{\partial s}\bigg|_{s=0}, \\ \text{var}[\mathcal{Q}_{d,i}^b] &= -\frac{\partial^2 \mathcal{L}_{\mathcal{Q}_{d,i}^b}(s)}{\partial s^2}\bigg|_{s=0} - \left(\mathbb{E}\big[\mathcal{Q}_{d,i}^b\big]\right)^2 \end{aligned}$$

where $\mathcal{L}_{\mathcal{Q}_{d,i}^b}(s)$ is the Laplace transform of $\mathcal{Q}_{d,i}^b$ and $R_c = 1/2\sqrt{\lambda_1}$ is the cell radius. Means and variances of $\mathcal{Q}_{d,i}^m$, $\mathcal{Q}_{r,i}$ can be calculated similarly. □

From the above results for interference power statistics, the interference power is directly proportional to both the active users density, λ_1 , and the transmission power levels represented by $\zeta_i, i \in [1:4]$ in Eqs. 1.34 - 1.37

1.5.2 Modelling Interference Power Distribution

A parameterized probability distribution, which includes a wide variety of curve shapes, is useful in the representation of data when the underlying model is unknown or difficult to obtain in closed form. A parameterized probability distribution is usually characterized by its flexibility, generality, and simplicity. Although distributions are not necessarily determined by their moments, the moments often provide useful information and are widely used in practice. It is shown that the Gamma distribution is a good approximation

for the interference when the point under study is closer to the cell center, but fails to represent the actual interference distribution whenever the point under study is exactly at the cell edge. We use the same approach here and match a Gamma distribution to the first two moments of the interference power terms derived earlier in Theorem 1.2.

Gamma Distribution

The Gamma distribution is specified by a shape parameter k and a scale parameter θ. The pdf of a Gamma distributed RV $\gamma[k, \theta]$ is defined as

$$F_\gamma(q|k, \theta) = \frac{q^{k-1}e^{(-q/\theta)}}{\theta^k \Gamma(k)}$$

where the Gamma function $\Gamma(t)$ is defined as $\Gamma(t) = \int_0^\infty x^{t-1}e^{-x}dx$. The mean and variance of $\gamma[k, \theta]$ are $k\theta$ and $k\theta^2$ respectively.

Since we know mean and variance of interference powers, we can estimate the shape and scale parameters by using the formulae:

$$k_i = \frac{(\mathbb{E}[\mathcal{Q}_i])^2}{\text{var}[\mathcal{Q}_i]}, \theta_i = \frac{\text{var}[\mathcal{Q}_i]}{\mathbb{E}[\mathcal{Q}_i]} \tag{1.38}$$

1.6 Simulations and Results

1.6.1 Simulation Setting

All simulations were done on a square region of side length 200m. To generate active UEs in the region, the number of UEs is taken as a realization of poisson RV with parameter λ_1 and these number of UEs were uniformly distributed in the square region. The same is done to generate idle UEs but with parameter λ_2. I discarded the UEs whose Voronoi region extends to infinity.

In theory, the base station of a UE is uniformly distributed in the Voronoi region of UE but there is no easy practical way to uniformly pick a point from a polygonal area. One method is to triangulate the polygonal Voronoi region, choose a triangle weighted by area, choose a point inthat triangle. This is clearly quite complex to code so I've not implemented this method. The method I followed to generate BSs is - pick a number greater than or equal to the number of active UEs and distribute these number of BSs uniformly in the square region. Now go to each active UE and check if there are any BSs

in its Voronoi region. If there are BSs, pick one of them and associate it with the UE and discard other BSs in the Voronoi region. Since BSs are distributed uniformly over the whole region, the result is as good as picking BSs uniformly in the Voronoi regions of UEs which is what we wanted but there is a catch. In the theoritical method, each UE with a finite Voronoi region is guaranteed to have a BS whereas in the way that I'm generating, some UEs might not have a BS even though their Voronoi region is of finite area. Further, the UEs without a BS are not included in rate or cooperation probability analysis which is logical since without an associated BS, the UEs cannot considered active.

For all simulations, we assume that UEs are using maximum power to transmit without applying any power control method. The powers used during the two phases of transmission are as follows

- Source and relays use equal power $\Rightarrow P_{s,i} = P_{r,i}$
- Source use equal power during broadcast and multicast phases $\Rightarrow P^{b}_{s,i} = P^{m}_{s,i}$
- $P^{m_1}_{s,i} = \beta_1 P^{m}_{s,i}$ and $P^{m_2}_{s,i} = (1-\beta_1) P^{m}_{s,i}$. Where β_1 is allocated optimally to maximize the transmission rate of the active user. To do this, rate is expressed as a function of β_1 and minimized negative rate using MATLAB tool *fminrnd*.

1.6.2 Results

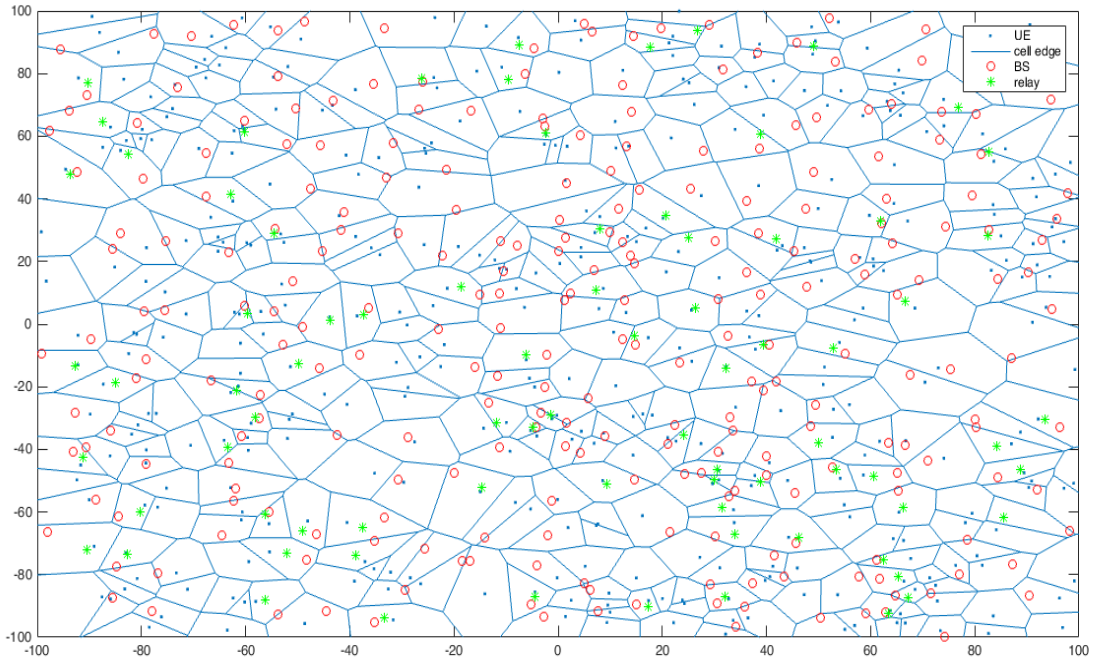

Figure 1.3: Network Layout

This a sample network layout generated by using the method discussed in previous subsection. We can see that some of the UEs are well within the range but have no BS. Only UEs with a BS are considered active. A fraction active UEs have relays, these UEs use PDF relaying. Cooperation probability = number of active UEs with relays/total number of active UEs.

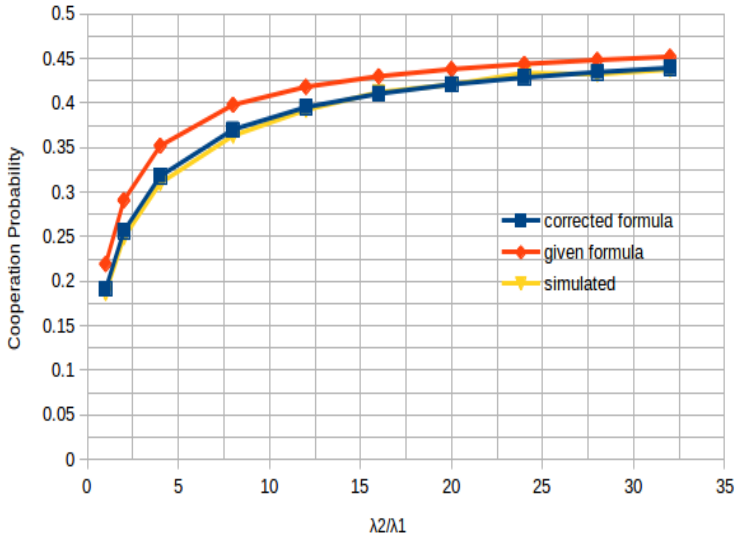

Figure 1.4: Corrected cooperation probability of E_3

In the published paper, the analytic result for cooperation probability of E_3 has an error. The correction being using $\mathcal{E}_3$ instead of $\mathcal{E}_2$ in eq. 1.26. The corrected analytic result matches the simulation result as can be seen in the above figure.

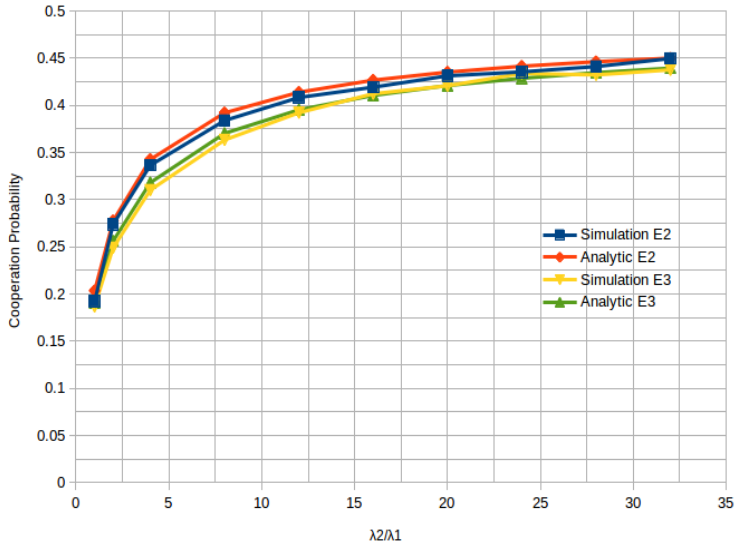

Figure 1.5: Cooperation probabilities of E_2, E_3 versus user density ratio

From the above graph we can see that cooperation probability of both policies increases with user density ratio(λ_2/λ_1) and reach a maximum of 0.5 for very large user density ratio. Also, the analytic and simulations results closely match.

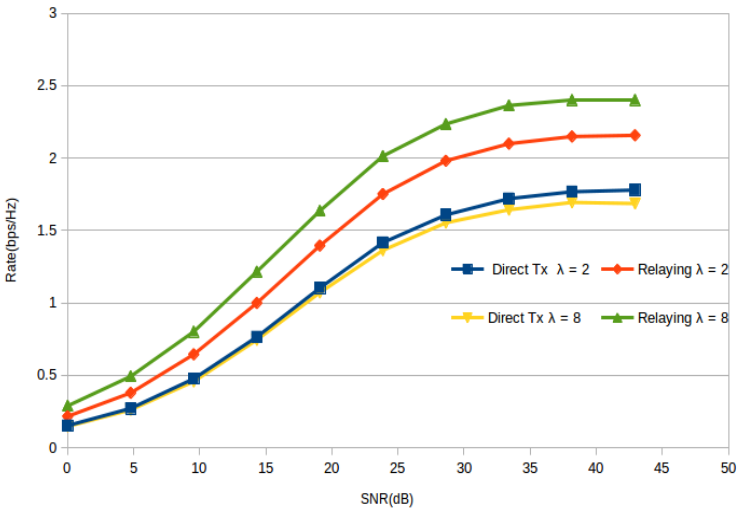

Figure 1.6: Average rate per user; $\lambda = \lambda_2/\lambda_1$

From the above figure, we can clearly see that average rate per user has increased when PDF relaying is deployed over the whole network. The rate also increases as user density ratio is increased but we caan't sure whether the rate keeps increasing with λ. It might happen that the rate decreases for very large user ratio density due to increase in interference.

1.7 Future Work

- Analysis and Simulation of a new policy E_4. In the two policies discussed in earlier sections, only the first neighbour of the active UE is seen as a potential relay. But intuitively any relay that satisfies the conditions mentioned in E_2 should be good enough. This also means higher cooperation probability, shown in figure 1.7 and high inteference. If the inteference is so high that the rate decreases for some users, then there should be a way of deciding which users should use the relaying so that rate will be high for all users. need to be done using the new policy and if is promosing in terms per user average rate, then an analytic expression for cooperation probability should be developed.

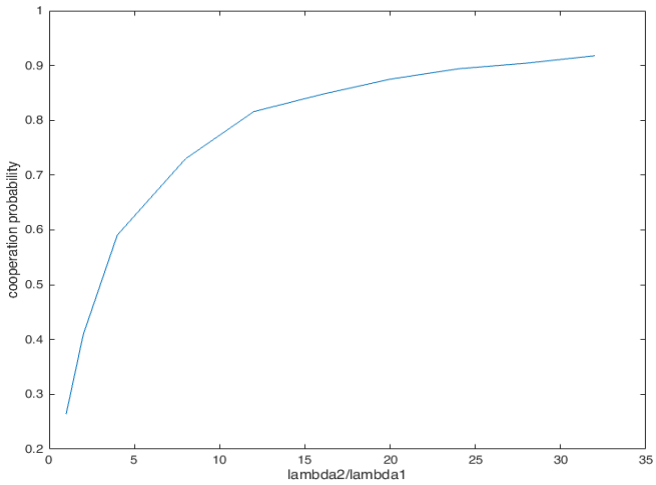

Figure 1.7: Cooperation probability in E4 versus user density ratio

- As mentioned in section 1.6.1, the UEs are not using any power control techniques while deciding the transmission power. In practice, UEs use power control techniques which in essence reduce the transmission power when the UE is closer to the BS and use maximum power when the mobile phone is at the cell edge. This reduces the interference and can increase the data rate.

- To determine how much power needs to be allocated to transmit the common codeword in second phase i.e., $P_s^{m_1}$, we are optimizing rate with respect to $P_s^{m_1}$ but this is not practical. UEs should know before hand how much power should be pumped to transmit the codeword. An algorithm needs to be developed that estimates $P_s^{m_1}$ based on channed conditions.

Chapter 2

Joint reconstruction from multiple observations

In the previous chapter we saw that the problem is to determine the image(i.e intensity distribution) from an incomplete set of Fourier measurements since we have data available only at certain points in the Fourier domain, determined by the $u - v$ coverage of the antenna setup. In general we assume that we have data available at points in the Fourier domain determined by the "sampling map". Next we present the problem formulation.

2.1 Problem Formulation

We consider the problem where we have two incomplete sets of Fourier measurements corresponding to two different images and further we have knowledge about some information overlap between the two images. We want to make use of this overlapping information to perform simultaneous recovery of both images. Next we formulate the simultaneous recovery problem,

Let x and y be the discretized vectors of the lexicographic ordering of the intensity distributions (i.e. the images) of size $N \times 1$. Corresponding to each image we have a set of linear measurements obtained as,

$$b_x = \Phi_x x + n_x \tag{2.1}$$

$$b_y = \Phi_y y + n_y, \tag{2.2}$$

where Φ_x and Φ_y are $M_x \times N$ and $M_y \times N$ measurement matrices respectively and n_x

and n_y are terms corresponding to the noise added to the system while obtaining the measurements ($M_x < N,\ M_y < N$).

Let both x and y be sparse/compressible in the same basis and thus they can be represented as,

$$x = \Psi z_x \tag{2.3}$$

$$y = \Psi z_y, \tag{2.4}$$

where z_x and z_y are $N \times 1$ sized vectors containing only few non-zero/large coefficients and Ψ is the $N \times N$ matrix with columns as the basis vectors of the desired basis.

Let there be some information overlap between x and y. We will restrict ourselves to only those features that can be extracted through a linear operation on the images. Let f_x and f_y be the $S \times 1$ feature vectors obtained from x and y as,

$$f_x = B_x z_x \tag{2.5}$$

$$f_y = B_y z_y, \tag{2.6}$$

where B_x and B_y are $S \times N$ feature extraction matrices. For example if the last c columns of image corresponding to x overlap with the first c columns of the image corresponding to y then B_x and B_y will be $cn \times N$ matrices where we assume the images to be of size $n \times n$ and $N = n^2$. B_x and B_y will have rows with all entries zero except the position corresponding to the location of a certain pixel in the lexicographic ordering of the image. Under ideal reconstruction, the two feature vectors must match because they correspond to the overlapping part.

$$||f_x - f_y||_2^2 < \epsilon_f, \tag{2.7}$$

where ϵ_f is some tolerance threshold. Next we present several formulations that can be used to solve this problem:

1. **Formulation-1** Using conventional compressed sensing methods, we will first solve for z_x^* and z_y^* independently as follows and obtain x^* and y^* using (2.3) and (2.4):

$$z_x^* = \arg\min_{z_x} \|z_x\|_1 \text{ for } \|\Phi_x \Psi z_x - b_x\|_2^2 \leq \epsilon_x \tag{2.8}$$

$$z_y^* = \arg\min_{z_y} \|z_y\|_1 \text{ for } \|\Phi_y \Psi z_y - b_y\|_2^2 \leq \epsilon_y, \tag{2.9}$$

where ϵ_x and ϵ_y are variances corresponding to n_x and n_y respectively.

2. **Formulation-2** There is an alternative formulation which allows for unconstrained optimization.

$$z_x^* = \arg\min_z F(z) \equiv \|\Phi_x \Psi z - b_x\|_2^2 + \lambda_x \|z\|_1 \quad (2.10)$$

$$z_y^* = \arg\min_z F(z) \equiv \|\Phi_y \Psi z - b_y\|_2^2 + \lambda_y \|z\|_1, \quad (2.11)$$

where λ_x and λ_y must be chosen appropriately to obtain same results as obtain using *formulation-1*. Greedy methods such as ISTA and FISTA make use of this formulation to solve the problem.

3. **Formulation-3** Instead of solving for x and y separately we can solve for them simultaneously making use of the information overlap by the following formulation for unconstrained optimization,

$$z_x^*, z_y^* = \arg\min_{z_x, z_y} F(z_x, z_y), \quad (2.12)$$

where,

$$F(z_x, z_y) \equiv \|\Phi_x \Psi z_x - b_x\|_2^2 + \|\Phi_y \Psi z_y - b_y\|_2^2 + \lambda_x \|z_x\|_1 + \lambda_y \|z_y\|_1 + \mu ||f_x - f_y||_2^2. \quad (2.13)$$

Here, we have the four terms present from Formulation-2 but in addition we have a "*coupling term*" $||f_x - f_y||_2^2$ along with the "*coupling parameter*" μ. The parameter μ will decide the degree of overlap in the reconstructed images and setting $\mu = 0$ will revert back to Formulation-2. Here λ_x, λ_y and μ must be chosen appropriately to ensure convergence to correct results. We propose an alternating algorithm to solve this optimization problem which is in similar lines to the ISTA or FISTA algorithm in one argument. This formulation reduces to the formulation JSM-1 presented in [9] when $B_x = B_y$, but with a subtle difference. In the formulation presented in [9] the common part has to be same at every iteration of the algorithm but in our formulation we allow the common part in both images to take different values during the course of the algorithm but reach close to being same at convergence depending upon the weight μ.

2.2 Alternating Algorithm for Simultaneous Recovery

The alternating algorithm is a generalization of the ISTA which is a proximal gradient algorithm. We first briefly look at proximal methods and then the ISTA and FISTA algorithm and finally present the alternating algorithm.

2.2.1 Proximal Methods

Proximal methods are a higher level of abstraction than classical optimization algorithms such as gradient descent. The basic constituent of a proximal method is the *proximal operator*, which essentially solves a simple convex optimization problem [10]. The proximal operator for the scaled function f at a point x with respect to parameter λ is given by,

$$prox_{\lambda f}(x) = \arg\min_{y} \left(f(y) + \frac{1}{2\lambda}\|x - y\|^2. \right) \tag{2.14}$$

We refer to $prox_{\lambda f}(x)$ as the proximal operator of f with respect to parameter λ at point x. Here the $\|\|x - y\|\|^2$ term keeps the mapped point in the proximity of the argument x and the $\min f(y)$ term, drives the mapped point towards the minima of the function f. The parameter λ decides which of the two factors dominates.

Figure 2.1: Effect of the Proximal Operator [1]

[1]Image Source: `http://www.stanford.edu/~boyd/papers/pdf/prox_algs.pdf`

Consider the figure 2.1. Here, the proximal operator maps the blue points to the red points. The mapped points come closer to the minima, but still remain in proximity of the original blue point.

2.2.2 Proximal operator for smooth functions

1. Consider a smooth function $f(x)$.

2. The proximal operator for f with respect to parameter t at point x is given by:

$$prox_{tf}(x) = \arg\min_y \left(f(y) + \frac{1}{2t}\|x-y\|^2 \right). \tag{2.15}$$

   As, the mapped point is expected to be in the proximity of the original point x, we use a linear approximation of $f(y)$ at x and thus we have,

$$prox_{tf}(x) = \arg\min_y \left(f(x) + (y-x)^T \nabla f(x) + \frac{1}{2t}\|x-y\|^2 \right). \tag{2.16}$$

3. On simplification, we obtain:

$$prox_{tf}(x) = \arg\min_y \left(\frac{1}{2t}\|y - (x - t\nabla f(x))\|_2^2 \right). \tag{2.17}$$

   Thus for smooth convex functions,

$$prox_{tf}(x) = (x - t\nabla f(x)) \tag{2.18}$$

4. Note that this is the exact gradient step for stepsize t, in the gradient descent method. Thus, one can interpret the proximal algorithms as a generalization of gradient descent algorithms.

Proximal operator for l_1 norm

We next consider the proximity operator for the l_1 norm function.

1. Let the l_1 norm function be $g(x)$,

$$g(x) = \|x\|_1 = \sum_{i=1}^{n} |x_i| \tag{2.19}$$

2. From [10], the proximal operator for g with respect to parameter α at point x is given by :

$$prox_{\alpha g}(x) = (|x_i| - \alpha)_+ sgn(x_i) \tag{2.20}$$

Here, $sgn(x)$ is the standard signum function.

3. The $(z)_+$ function takes the maximum of z and 0:

$$(z)_+ = z, \quad z \geq 0 \tag{2.21}$$

$$= 0, \quad z < 0. \tag{2.22}$$

2.2.3 The ISTA Algorithm

The ISTA, Iterative Shrinkage and Thresholding Algorithm [11] is a proximal gradient algorithm, which is used to minimize the functions of the kind:

$$F(x) = f(x) + g(x) \tag{2.23}$$

1. $x \in \mathbb{R}^n$, $f(x)$ is a smooth convex function, while the function $g(x)$ is convex but non-smooth.

2. First derivative of $f(x)$ satisfies a Lipschitz conditon with constant L, i.e.

$$\|f^{(1)}(x) - f^{(1)}(y)\|_2 \leq L\|x - y\|_2. \tag{2.24}$$

3. Starting from an initial point x^0 we apply the proximity operator on functions $f(x)$ and $g(x)$ successively to obtain the next iterate [12],

$$x^{k+1} = prox_{\lambda tg}(prox_{tf}(x^k)). \tag{2.25}$$

4. Since $f(x)$ is smooth, from (2.18),

$$x^{k+1} = prox_{\lambda tg}\left(x^k - t\nabla f(x^k)\right). \tag{2.26}$$

5. Note, that the step size t is chosen as $\frac{1}{L}$, and the proximity parameter λ for $g(x)$

needs to be chosen appropriately, for the algorithm to work correctly and also be fast enough.

The pseudo-code for the ISTA algorithm is given below:

ISTA pseudo-code

We only consider the ISTA algorithm for a fixed stepsize. For a backtracking variant, and more information on the standard implementation, please refer to [11]

Algorithm 1: ISTA with constant stepsize

Data: initial value x^0, L, λ

Result: Finds the global minimum for the objective function $F(x)$

$k = 0$;

$t = \frac{1}{L}$;

repeat

$x^{k+1} := prox_{\lambda tg}\left(x^k - t\nabla f(x^k)\right)$;

$k := k + 1$;

until *iterate not converged*;

The stopping criteria used for the algorithms is:

$$\left|\frac{F(x^k) - F(x^{k-1})}{F(x^{k-1})}\right| \leq \epsilon \tag{2.27}$$

1. The convergence rate for the algorithm goes as $\mathcal{O}(1/k)$. For the complete proof, please refer to [11].

2. Note that ISTA is a monotonically converging algorithm, i.e. in every step, the value of the objective function decreases.

We next have a look at the FISTA algorithm.

2.2.4 The FISTA Algorithm

The FISTA, Fast Iterative Shrinkage and Thresholding Algorithm [11] is a proximal gradient algorithm , which is used to minimize the functions of the kind similar to those in ISTA:

$$F(x) = f(x) + g(x) \tag{2.28}$$

1. $x \in \mathbb{R}^n$, $f(x)$ is a smooth convex function, while the function $g(x)$ is convex but non-smooth.

2. First derivative of $f(x)$ satisfies a Lipschitz conditon with constant L.

3. The FISTA algorithm operates very similar to the ISTA algorithm, but includes an 'extrapolation' step, as below:

$$y^{k+1} = x^k + w_{k+1}(x^k - x^{k-1}) \tag{2.29}$$

$$x^{k+1} = prox_{\lambda t g}(y^{k+1} - t\nabla f(y^{k+1})); \tag{2.30}$$

4. In FISTA, the gradient and the proximity operator for g are not applied at the iterate x^k, but at a extrapolated point y^{k+1}, formed by a specific linear combination of $\{x^k, x^{k-1}\}$.

5. Note that the parameters w_i need to be chosen appropriately to ensure convergence and obtain good performance.

FISTA pseudo-code

We only consider the FISTA algorithm for a fixed stepsize. For a backtracking variant, and more information on the standard implementation, please refer to [11]

The stopping criteria for the algorithm is:

$$\left| \frac{F(x^k) - F(x^{k-1})}{F(x^{k-1})} \right| \leq \epsilon \tag{2.31}$$

Algorithm 2: FISTA with constant stepsize

Data: initial value x^0, L, λ

Result: Finds the global minimum for the objective function $F(x)$

$k = 0$;

$t = \frac{1}{L}$;

$u^1 = 1$;

$y^1 = x^0$;

repeat

$k := k + 1$;

$x^k := prox_{\lambda t g}(y^k - t\nabla f(y^k))$;

$u^{k+1} = \frac{1+\sqrt{1+4(u^k)^2}}{2}$;

$y^{k+1} = x^k + \left(\frac{u^k - 1}{u^{k+1}}\right)(x^k - x^{k-1})$

until *iterate not converged*;

1. If the parameters are chosen in the way mentioned above, it can be shown that the covergence rate for the algorithm is $\mathcal{O}(1/k^2)$. [11]

2. Also, as opposed to ISTA, FISTA is not a monotonically covergent algorithm. This implies that, the objective function might not decrease in during every iteration, but globally it does decrease.

3. Direct application of ISTA and FISTA to reconstruct images has been explored in literature and the range of λ for good performance has been explored in the dual degree dissertation by Kedar Tatwawadi, IIT B [13]. Next we present two variants of an alternating algorithm based on ISTA and FISTA respectively to perform joint minimization based on Formulation-3.

2.3 ISTA based Alternating Algorithm for Joint Minimization

1. The function we wish to minimize with respect to z_x and z_y is,

$$F(z_x, z_y) = \|\Phi_x \Psi z_x - b_x\|_2^2 + \|\Phi_y \Psi z_y - b_y\|_2^2 + \lambda_x \|z_x\|_1 + \lambda_y \|z_y\|_1 + \mu ||f_x - f_y||_2^2. \quad (2.32)$$

2. Let the smooth part of the above function be,

$$f(z_x, z_y) = \|A_x z_x - b_x\|_2^2 + \|A_y z_y - b_y\|_2^2 + \mu||C_x z_x - C_y z_y||_2^2. \tag{2.33}$$

3. We will start will initial guesses for z_x and z_y and will update z_x and z_y iteratively alternating between iterations on z_x and z_y.

4. At the k^{th} iteration on z_x we will find the update z_x^{k+1} by treating $f(z_x, z_y)$ as a function of z_x alone with z_y as a constant taking value z_y^k.

5. Let $f_x^k(z_x) = f(z_x, z_y^k)$. Then we update z_x as in the ISTA algorithm where the smooth part now is $f(z_x) = f_x^k(z_x)$ and the non differentiable part is $g(z_x) = \lambda_x \|z_x\|_1$.

$$z_x^{k+1} := prox_{\lambda_x t_x g}\left(z_x^k - t_x \nabla_{z_x} f(z_x^k, z_y^k)\right), \tag{2.34}$$

where $\nabla_{z_x} f(z_x^k, z_y^k) = \nabla_{z_x} f_x^k(z_x^k)$ based on definition of $f_x^k(z_x)$.

6. At the k^{th} iteration on z_y we will find the update z_y^{k+1} by treating $f(z_x, z_y)$ as a function of z_y alone with z_x as a constant taking value z_x^{k+1}.

7. Let $f_y^k(z_y) = f(z_x^{k+1}, z_y)$. Then we update z_y as in the ISTA algorithm where the smooth part now is $f(z_y) = f_y^k(z_y)$ and the non differentiable part is $g(z_y) = \lambda_y \|z_y\|_1$.

$$z_y^{k+1} := prox_{\lambda_y t_y g}\left(z_y^k - t_y \nabla_{z_y} f(z_x^{k+1}, z_y^k)\right), \tag{2.35}$$

where $\nabla_{z_y} f(z_x^{k+1}, z_y^k) = \nabla_{z_y} f_y^k(z_y^k)$ based on definition of $f_y^k(z_x)$.

8. Note, that the step size t_x and t_y are chosen as $\frac{1}{L_x}$ and $\frac{1}{L_y}$ respectively where L_x and L_y are the upper bounds on Lipschitz constants for $f_x^k(z_x)$ and $f_y^k(z_y)$ over all k.

9. The parameters λ_x, λ_y and μ need to be chosen appropriately, for the algorithm to converge to desired solution and also be fast enough. If λ_x is too low then we will not move away from initial solution and if λ_x is too high we will converge to the all zero solution.

10. If μ is too low we will get similar results as for the case where we solve the minimization problem separately for z_x and z_y and if μ is too high then we may not get sparse solutions.

2.3.1 ISTA based alternating algorithm pseudo-code

The pseudo code for the ISTA based alternating algorithm is given below. The stopping criteria for the algorithm is:

$$\left| \frac{F(z_x^{k+1}, z_y^{k+1}) - F(z_x^k, z_y^k)}{F(z_x^k, z_y^k)} \right| \leq \epsilon \tag{2.36}$$

Algorithm 3: ISTA based alternating algorithm

Data: initial values $z_x^0, z_y^0, L_x, L_y, \lambda_x, \lambda_y, \mu$

Result: Finds the global minimum for the objective function $F(z_x, z_y)$

$k = 0$;

$t_x = \frac{1}{L_x}$;

$t_y = \frac{1}{L_y}$;

repeat

$z_x^{k+1} := prox_{\lambda_x t_x g}\left(z_x^k - t_x \nabla_{z_x} f(z_x^k, z_y^k)\right)$;

$z_y^{k+1} := prox_{\lambda_y t_y g}\left(z_y^k - t_y \nabla_{z_y} f(z_x^{k+1}, z_y^k)\right)$;

$k := k + 1$;

until *iterate not converged*;

2.4 FISTA based Alternating Algorithm for Joint Minimization

1. The FISTA based alternating algorithm is very similar to the ISTA based algorithm and is used in similar settings.

2. In this variant before updating z_x we perform an 'extrapolation step' as follows,

$$q_x^{k+1} = z_x^k + w_{k+1}(z_x^k - z_x^{k-1}) \tag{2.37}$$

$$z_x^{k+1} = prox_{\lambda_x t_x g}\left(q_x^{k+1} - t_x \nabla_{z_x} f(q_x^{k+1}, z_y^k)\right). \tag{2.38}$$

3. Similarly before updating z_y we do the following,

$$q_y^{k+1} = z_y^k + w_{k+1}(z_y^k - z_y^{k-1}) \tag{2.39}$$

$$z_y^{k+1} = prox_{\lambda_y t_y g}\left(q_y^{k+1} - t_y \nabla_{z_y} f(z_x^{k+1}, q_y^{k+1})\right). \tag{2.40}$$

4. Note that the parameters w_i need to be chosen appropriately to ensure convergence and obtain good performance.

2.4.1 FISTA based alternating algorithm pseudo-code

The pseudo code for the FISTA based alternating algorithm is given below. The stopping criteria for the algorithm is same as in the ISTA variant.

Algorithm 4: FISTA based alternating algorithm

Data: initial values $z_x^0, z_y^0, L_x, L_y, \lambda_x, \lambda_y, \mu$

Result: Finds the global minimum for the objective function $F(z_x, z_y)$

$k = 0$;

$u^1 = 1$;

$q_x^1 = z_x^0$;

$q_y^1 = z_y^0$;

$t_x = \frac{1}{L_x}$;

$t_y = \frac{1}{L_y}$;

repeat

$k := k + 1$;

$z_x^k := prox_{\lambda_x t_x g}\left(q_x^k - t_x \nabla_{z_x} f(q_x^k, z_y^k)\right)$;

$z_y^k := prox_{\lambda_y t_y g}\left(q_y^k - t_y \nabla_{z_y} f(z_x^{k+1}, q_y^k)\right)$;

$u^{k+1} = \frac{1+\sqrt{1+4(u^k)^2}}{2}$;

$q_x^{k+1} = z_x^k + \left(\frac{u^k - 1}{u^{k+1}}\right)(z_x^k - z_x^{k-1})$;

$q_y^{k+1} = z_y^k + \left(\frac{u^k - 1}{u^{k+1}}\right)(z_y^k - z_y^{k-1})$

until *iterate not converged*;

In the next chapter we use the above algorithms to perform simultaneous recovery for various classes of images. We compare the performance using the joint reconstruction with that obtained using independent reconstructions.

Chapter 3

Conclusion and Further Work

3.1 Conclusion

Based on the results and observations from the experiments conducted we conclude the following:

1. When we have incomplete Fourier measurements of two images that are sparse in some domain, and we have "information overlap" present between the two images, we presented a coupled framework that performs joint minimization to recover both images simultaneously.

2. To perform the reconstruction we presented two variants of the alternating algorithm inspired by the ISTA and FISTA algorithm respectively.

3. We consider images that are sparse in spatial domain, images that are sparse in wavelet domain, and images that have both spatial doman sparse component and wavelet domain sparse components.

4. We compared the performance using the coupled framework with that while using the uncoupled framework on all classes of images and observed that the coupled framework that performs joint minimization to simultaneously solve for left and right images using the alternating algorithm performs better than the uncoupled framework that solves for each image independently.

5. While performing reconstruction in the coupled framework, we are making use of the information overlap present in the two images which is not done while using

the uncoupled framework.

6. In the scenario where the left and right images have different number of Fourier measurements available then while using the coupled framework the improvement in the image having lower number of measurements is much higher than the improvement in the one having higher number of measurements.

7. If the difference in the number of such measurements available is too large then the reconstruction of the image with higher number of measurements may actually deteriorate. We presented a heuristic to tackle this problem and achieve improvement in reconstruction error even in this case.

8. We focused on mainly astronomical images but this framework may also work on medical images as suggested by the peformance on the Shepp-Logan phantom.

3.2 Further Work

In this project, we presented an alternating algorithm for simultaneous recovery of multiple images from incomplete Fourier data when there is an information overlap present between the two images. There are several issues that are left unaddressed and can be looked at in the future.

1. **Alternating algorithm parameters and convergence**

   The alternating algorithm requires us to choose the parameters λ_x, λ_y and μ appropriately to obtain good performance. We chose these parameters by performing a range search along with a few heuristics. A theoretical approach to determine the parameters that give good performance is desirable. We have proofs of convergence of the ISTA and FISTA algorithm that the alternating algorithm is based on. Based on the ideas in these proofs, proof of convergence for the alternating algorithm can be derived. For the formulation where image is treated as sum of wavelet sparse and spatial domain sparse components we have given equal weight to the wavelet coefficients and pixel values by choosing $\lambda_x^s = \lambda_x^w$. This assumption can be relaxed to give different weights to the two sets of coefficients.

2. **Comparing performance with existing algorithms**

   As discussed previously, our formulation reduces to the formulation JSM-1 in [9]

when the two images are the sum of a common sparse component along with different sparse innovations, but with a subtle difference. The performance of our alternating algorithm can be compared against the algorithm mentioned in [14] to investigate if there is any improvement.

3. **Other classes of images**

   We restricted our attention to images of astronomical sources and the Shepp-Logan phantom. But our framework can also be used for other classes of images such as medical images where the image is sparse in some domain and we have an incomplete set of Fourier measurements.

Bibliography

[1] E. Candes and J. Romberg, "Quantitative robust uncertainty principles and optimally sparse decompositions," *Foundations of Computational Mathematics, 2006.*

[2] E. Candes, J. Romberg, and T. Tao, "Robust uncertainty principles:exact signal reconstruction from highly incomplete frequency information," *Information Theory IEEE, 2006.*

[3] E. Candes, J. Romberg, and T. Tao, "Stable signal recovery from incomplete and inaccurate measurements," *Communications on Pure and Applied Mathematics, 2006*, vol. 59.

[4] R. University, "Single pixel camera." http://dsp.rice.edu/cscamera.

[5] "Compressed sensing resources." http://dsp.rice.edu/cs.

[6] M. Davenport, M. Duarte, Y. Eldar, and G. Kutyniok, *Compressed Sensing: Theory and Applications.* 2012.

[7] S. Vignesh, "Compressed sensing for radio astronomy." Dual Degree Dissertation Stage I.

[8] TIFR, "Gmrt telescope." `http://gmrt.ncra.tifr.res.in/`.

[9] D. Baron, M. F. Duarte, M. B. Wakin, S. Sarvotham, and R. G. Barniuk, "Distributed compressive sensing." `http://arxiv.org/pdf/0901.3403.pdf`, 2009.

[10] N. Parikh and S. Boyd, "Proximal algorithms," *Foundations and Trends in Optimization, 2013*, vol. 1.

[11] M. Teboulle and A. Beck, "A fast iterative shrinkage-thresholding algorithm for linear inverse problems," *SIAM Journal on Imaging Sciences, 2009.*

[12] P. L. Combettes and J. C. Pesquet, "Proximal splitting methods in signal processing," *Springer, 2011.*

[13] K. Tatwawadi, "Compressed sensing for group testing and radio astronomy." Dual Degree Dissertation.

[14] D. Baron, M. F. Duarte, M. B. Wakin, S. Sarvotham, and R. G. Barniuk, "Distributed compressive sensing," tech. rep., Department of Electrical and Computer Engineering Rice University, 2005.